Carbohydrate Polymers 144 (2016) 362–370

Contents lists available at ScienceDirect

Carbohydrate Polymers

journal homepage: www.elsevier.com/locate/carbpol

Dermatan sulfate/chitosan polyelectrolyte complex with potential application in the treatment and diagnosis of vascular disease

Rita Y. Rasente[a,1], Julieta C. Imperiale[b,e,1], Juan M. Lázaro-Martínez[c,e], Luciana Gualco[a], Roxana Oberkersch[a,e], Alejandro Sosnik[d], Graciela C. Calabrese[a,*]

[a] Department of Biological Sciences, School of Pharmacy and Biochemistry, University of Buenos Aires, Junín 956, C1113AAD Ciudad Autónoma de Buenos Aires, Argentina
[b] Department of Pharmaceutical Technology, School of Pharmacy and Biochemistry, University of Buenos Aires, Junín 956, C1113AAD Ciudad Autónoma de Buenos Aires, Argentina
[c] Department of Organic Chemistry, School of Pharmacy and Biochemistry, University of Buenos Aires, Junín 956, C1113AAD Ciudad Autónoma de Buenos Aires, Argentina
[d] Laboratory of Pharmaceutical Nanomaterials Science, Department of Materials Science and Engineering, Technion-Israel Institute of Technology Technion City, Haifa, Israel
[e] CONICET, Av. Rivadavia 1917, C1113AAD Ciudad Autónoma de Buenos Aires, Argentina

ARTICLE INFO

Article history:
Received 20 October 2015
Received in revised form 26 January 2016
Accepted 16 February 2016
Available online 2 March 2016

Keywords:
Low molecular mass dermatan sulfate
Chitosan
Polyelectrolyte complexes
Endothelial uptake
Vascular disease

ABSTRACT

Cardiovascular disease is the largest single cause of morbid-mortality in the world. However, there is still no pharmaceutical treatment that directly targets the blood vessel wall instead of just controlling the risk factors. Here, we produced polyelectrolyte complexes (PECs) by a simple and reproducible polyelectrolyte complexation method between low molecular mass dermatan sulfate (polyanionic polysaccharide) and chitosan (polycationic polysaccharide), and evaluated the cellular uptake by vascular endothelial cells. The composition and the composition homogeneity of PECs were confirmed by ^{13}C-CP-MAS spectroscopy and by polyacrylamide gel electrophoresis, respectively. The hydrodynamic radius, determined by dynamic light scattering, was 729 ± 11 nm. PECs were not cytotoxic for a murine heart endothelium-derived cell line. Fluorescent confocal microscopy showed the specific uptake of fluorescently-labeled PECs by endothelial cells when they were cultured alone or in the presence of macrophages. Overall, these findings confirmed the potential of these PECs for targeting different agents to the vessel wall in the prevention, diagnosis, and therapy of vascular disease.

1. Introduction

Cardiovascular disease is the largest single cause of morbid-mortality in the developed and developing world. The major underlying disease process is atherosclerosis, combined with the explosion in the rates of obesity and type 2 diabetes (Little, Chait, & Bobik, 2011). Atherosclerosis is the result of a complex interaction between lipoproteins, extracellular matrix components and cells of the vessel wall leading to the formation of a lesion known as an atherosclerotic plaque (Fogelstrand & Borén, 2012). Predisposing risk factors for atherosclerosis, which include hypertension, diabetes, smoking, and hypercholesterolemia, are all linked to endothelial dysfunction (Jackson, Poppitt, & Minihane, 2012; Lacroix, Des Rosiers, Tardif, & Nigam, 2012; Rajendran et al., 2013). Endothelial extracellular matrix remodeling and inflammation are key factors in the process of formation of the atherosclerotic plaque, known as atherogenesis.

Proteoglycans (PGs), produced by both endothelial and smooth muscle cells, play a pivotal role, through the glycosaminoglycans (GAG) that form them in matrix organization and modulation of the activity of growth factors and cytokines in the vascular wall (Neufeld et al., 2014). The expression and distribution of arterial PGs are significantly modulated during atherosclerosis and

Abbreviations: ^{13}C CP-MAS, high-resolution ^{13}C solid-state spectroscopy; CS, chitosan; Dh, size; DIC, differential interference contrast microscopy; DLS, dynamic light scattering; DMEM, Dulbecco's Modified Eagle Medium; DS, dermatan sulfate; ECs, endothelial cells; FBS, fetal bovine serum; FITC, fluorescein isothiocyanate; FITC-PECs, FITC-labeled PECs; GAG, glycosaminoglycans; H5V cells, polyoma middle T-transformed murine heart endothelium-derived cell line; LMMDS, low molecular mass DS; MMP2, matrix metalloproteinase-2; MTT, 3-(4,5-dimethylthiazol-2-yl)-2,-5-diphenyltetrazolium bromide; PAGE, polyacrylamide gel electrophoresis; PDI, size distribution; PECs, polyelectrolyte complex particles; PGs, proteoglycans; Raw 264.7, abelson murine leukemia virus-transformed cells; ss-NMR, solid-state Nuclear Magnetic Resonance; TNF-α, tumor necrosis factor-α; TPPM, two-pulse phase modulation; Z-potential, zeta potential.

* Corresponding author. Fax: +54 11 508 3645.
E-mail address: gcalabe@ffyb.uba.ar (G.C. Calabrese).
[1] These authors contributed equally to this work.

http://dx.doi.org/10.1016/j.carbpol.2016.02.046
0144-8617/

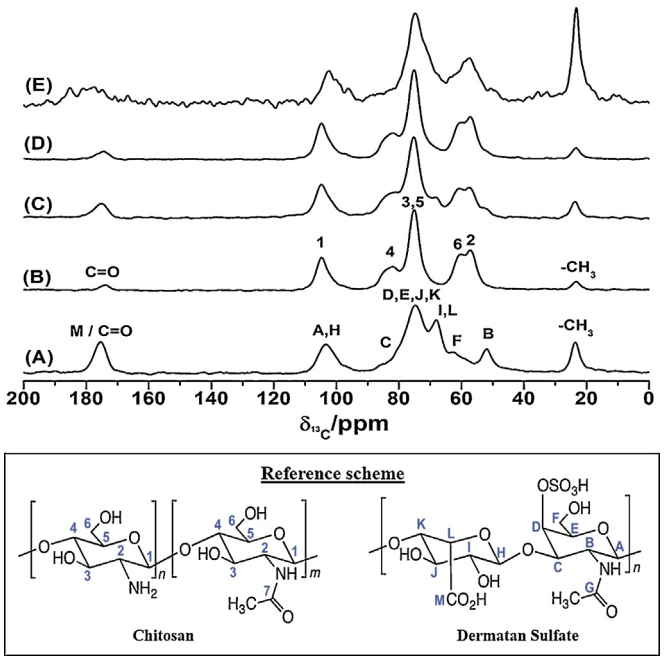

Fig. 1. ^{13}C CP-MAS spectra of (A) LMMDS, (B) CS, (C) physical blend of CS:LMMDS (1:1), (D) physical blend of CS:LMMDS (9:1) and (E) freeze-dried PECs. The numbering corresponds to the one presented in the Reference scheme, which shows the chemical structures of chitosan (CS) and dermatan sulfate (DS).

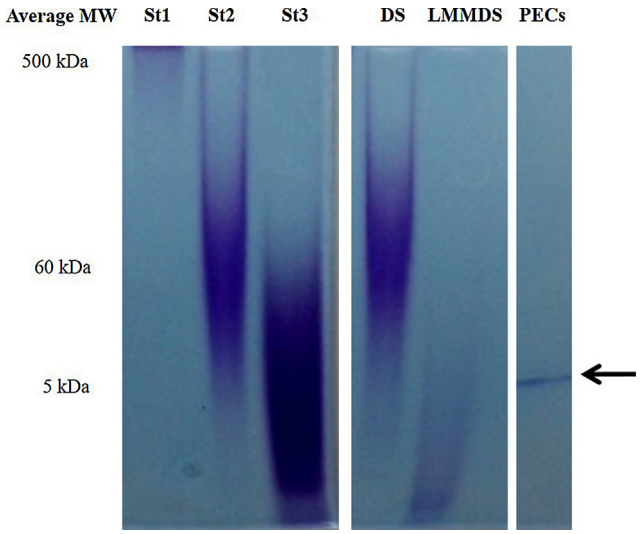

Fig. 2. Electrophoretic mobility of PECs. Samples of PECs were compared with standard polysaccharides of different molecular weights (St1 through St3) (10 μg of each) on 6% polyacrylamide gels in sodium barbital buffer (pH 8.6), after toluidine blue staining. St1 is high molecular dextran sulfate (average molecular mass = 500 kDa); St2 is chondroitin-6-sulfate from shark cartilage (average molecular mass = 60 kDa); St3 is low molecular weight dextran sulfate (average molecular weight = 5 kDa); DS is high molecular mass DS and LMMDS is low molecular mass DS. The well-defined band that corresponds to the PECs is indicated with an arrow.

aging (Oberkersch et al., 2014; Tovar, Cesar, Leta, & Mourao, 1998). Moreover, the prelesional distribution of PGs like biglycan and decorin in human coronary arteries from young subjects is similar to lipid distribution in the early phase of type I lesions, suggesting the key involvement of PGs in the process (Nakashima, Fujii, Sumiyoshi, Wight, & Sueishi, 2007). Besides, GAG chains attached to the protein core of PGs undergo specific structural modifications during the development of the disease; e.g., elongated GAG chains have been reported in early human atherosclerotic lesions (Little, Ballinger, & Osman, 2007; Theocharis, Theocharis, De Luca, Hjerpe, & Karamanos, 2002). For instance, hyperelongated chondroitin sulfate chains of biglycan may be crucial in atherosclerosis because they enhance the binding affinity of low density lipoproteins to the vascular wall (Anggraeni et al., 2011). Conversely, dermatan sulfate (DS) or chondroitin sulfate B, a polysaccharide formed by the assembly of disaccharide units containing a hexosamine, N-acetyl galactosamine or glucuronic acid linked by β 1,4 or 1,3 linkages respectively (Trowbridge & Gallo, 2002), could protect the arterial wall from atherogenesis. For example, DS chains greatly increase the rate of thrombin inhibition by Heparin Cofactor II. Since thrombin is thought to contribute to atherogenesis by influencing coagulation, chemoattraction and cell proliferation, DS would provide the tissue with antiatherogenic properties (Rasente, Egitto, & Calabrese, 2012; Tollefsen, 2010). Moreover, we have previously described that low molecular mass DS (LMMDS) induces the entrance of cells into the S phase of the cell cycle, enhances the activity of matrix metalloproteinase-2 (MMP2), and might modulate endothelial cell migration through mechanisms independent of tumor necrosis factor-α (TNF-α) (Rasente et al., 2012).

Current therapies target risk factors that contribute to increase the incidence of cardiovascular disease. The maximum efficacy of these approaches as determined from multiple clinical trials is limited to around 30% (Little et al., 2011). Notably, even though atherosclerosis occurs within the vessel wall, there is no pharmaceutical treatment that directly targets endothelial dysfunction or the blood vessel wall and is capable of preventing the atherosclerotic process.

Polyelectrolyte complexes (PECs) formed between polycations and polyanions have been extensively investigated for drug delivery (Luo & Wang, 2014), probably due to the fact that the spontaneous association of the oppositely-charged polymers leads to the formation of PECs through strong and reversible electrostatic links; the transient structure obtained avoids the use of toxic covalently bonded chemical cross-linkers, thus allowing them to be used in humans (Thakker et al., 2014). Ranney et al. (2005) reported that the tumor neovasculature is sufficiently more bioadhesive than normal endothelium to bind to a therapeutic agent formulated with DS and doxorubicin (Ranney et al., 2005). On the other hand, chitosan (CS) is a highly positive natural mucoadhesive polysaccharide that due to very good biocompatibility is being extensively investigated in a broad spectrum of biomedical applications (Sosnik, das Neves, & Sarmento, 2014). CS is non-toxic and it does not elicit allergic reactions; moreover, its degradation products (amino sugars) are metabolized by the human body (Agnihotri, Mallikarjuna, & Aminabhavi, 2004). In addition, CS is capable of PEC formation with polyanionic molecules, retaining its mucoadhesive properties and the ability to transiently disrupt tight junctions in different endothelia (Patel, Patel, & Patel, 2010; Wilson et al., 2010).

In this context, the present work aimed to investigate a novel platform based on the production of PECs made of CS and LMMDS, and investigate its cellular uptake by endothelial cells (ECs) toward their implementation in the prevention, diagnosis and therapy of vascular disease

2. Experimental

2.1. Materials

DS (PM 60 kDa) and LMMDS (PM 5 kDa) were a gift by Syntex S.A., Argentina. DS was extracted from bovine intestinal mucosa (Batch No. 082–91, Buenos Aires, Argentina); LMMDS was obtained by peroxy-radical molecular depolymerization from DS (Díaz, Dománico, & Fussi, 1990; Díaz, Dománico, & Fussi, 1993). Low molecular weight CS (viscosity 20–300 cps, deacetylation degree 95.5%, catalog number 448869), high molecular weight CS (viscos-

Table 1
Physical stability of CS-LMMDS PECs at room temperature based on D_h, PDI and Z-potential was evaluated as a function of time.

Time (Days)	D_h (nm) (±SD)				PDI (±SD)	Z-potential (mV) (±SD)
	Peak 1	%	Peak 2	%		
0	729 (11)	93.0	93 (4)	7.0	0.322 (0.055)	49.4 (0.8)
4	719 (41)	93.3	95 (1)	6.7	0.341 (0.023)	49.7 (0.3)
7	695 (80)	92.8	85 (6)	7.2	0.354 (0.037)	49.3 (0.8)
11	724 (79)	91.9	83 (26)	8.1	0.348 (0.048)	49.8 (1.6)
14	720 (85)	81.6	120 (38)	18.4	0.650 (0.045)	50.5 (1.7)

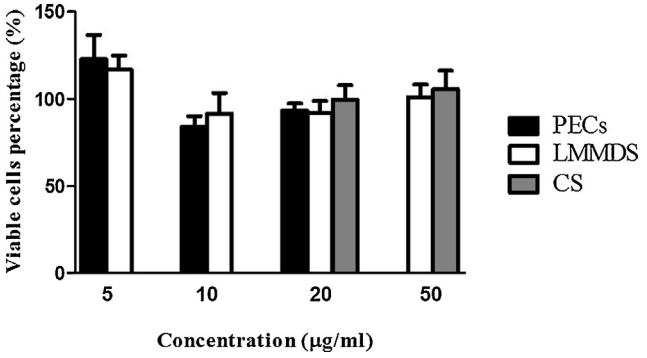

Fig. 3. MTT cytotoxicity assay. Percentage of viable H5V cells after incubation with CS, LMMDS, or PECs. H5 V cells were cultured in the absence or in the presence of increasing doses of LMMDS (0–50 μg/mL), CS (0–50 μg/mL), or PEC suspension (0–20 μg/mL, according to their LMMDS concentration), for 3 h. No statistical difference was observed in the number of viable cells with respect to the control after the addition of 5–20 μg/mL PECs. All experiments were performed in triplicate and results expressed as mean ± SD.

ity >400 cps, deacetylation degree 85%, catalog number 48165) and Dulbecco's Modified Eagle Medium (DMEM) were purchased from Sigma–Aldrich (St. Louis, MO, USA). Fetal bovine serum (FBS) was purchased from Natocor (Córdoba, Argentina). General reagents were of analytical grade or higher and used without further purification.

2.2. Chemical characterization and quantification of low molecular mass dermatan sulfate

The LMMDS concentration was determined by the reaction of carbohydrates with indole in HCl (Calabrese et al., 2004), and by metachromasy produced by sulfated GAGs with 1,9-dimethyl methylene blue (Calabrese, Gazzaniga, Oberkersch, & Wainstok, 2011).

2.3. Production of CS-LMMDS PECs

CS-LMMDS PECs were prepared by the PEC method of both CS types and LMMDS (Wen et al., 2012). Briefly, LMMDS was dissolved in distilled water (final concentration of 0.015% w/v) and the pH adjusted to 3.5 with 0.2 M HCl. Then, a CS solution in 2% v/v acetic acid water solution (pH adjusted to 3.5 with 0.1 M NaOH, final concentration of 0.050% w/v, 6 mL) was injected into the LMMDS solution (10 mL) using an infusion pump (flow of 40 mL/h, PC11U, APEMA S.R.L., Buenos Aires, Argentina) under constant magnetic stirring at room temperature. The suspension was stirred for 15 min after the end of the injection and filtered through a qualitative filter paper (Φ 125 mm, Xinxing, Fuyang, Zhejiang, China). The process was optimized by studying the effect of the molecular weight of CS on the particle size. All the experiments were performed in triplicate. Nanosuspensions were freshly used except for those that were subjected to a freeze-drying (48 h, Christ Freeze Dryer Unit GAMMA A, Martin Christ Gefriertrocknungsanlagen GmbH, Osterode am Harz, Germany) for compositional analysis.

Table 2
Elemental analysis of CS, LMMDS and PECs.

Material	%C	%H	%N	%S	S/N ratio
CS	38.80	7.62	6.67	–	–
LMMDS	26.73	4.78	2.24	4.82	2.15
PECs	30.53	5.34	5.09	0.97	0.19
PECs	30.53	5.34	5.09	0.97	0.19

CS-LMMDS PECs were also prepared employing CS labeled with fluorescein isothiocyanate (FITC) for the fluorescent experiments (Sarmento, Ribeiro, Veiga, & Ferreira, 2006). In brief, CS (50 mg) was dissolved in acetic acid (1% w/v, 5 mL) under constant magnetic stirring overnight. Then, methanol (5 mL) was added to the CS solution and stirred for 30 more min. A freshly prepared FITC methanolic solution (2 mg/mL, 3.2 mL) was consecutively added to the mixture and stirred for 3 h (in the dark), at room temperature. The resulting solution was precipitated with 1 M NaOH, centrifuged and rinsed with methanol until the free FITC could not be detected in the supernatant. The FITC-labeled CS was frozen and freeze-dried as described above.

2.4. Characterization of CS-LMMDS PECs

The size (D_h), size distribution (PDI) and zeta potential (Z-potential) of CS-LMMDS PECs was determined by dynamic light scattering (DLS) with a Zetasizer Nano ZS (Malvern Instruments, UK) equipped with a He–Ne (633 nm) laser and a digital correlator ZEN3600. The analysis was conducted at a scattering angle of 173° to the incident beam and a temperature of 25 °C. Results are expressed as the mean ± SD of at least three samples prepared under identical conditions and each one of them is the result of at least six runs. The physical stability of CS-LMMDS PECs was determined by storing the nanosuspension at room temperature over 14 days. Periodically, the D_h, PDI and Z-potential were measured by DLS as is detailed above. Measurements were performed by triplicate and results are expressed as the mean ± SD.

2.5. Elemental analysis

To determine the percentage (% w/w) composition of C, H, N and S, samples were analyzed by elemental analysis in a CE440 Elemental Analyser device (Exeter Analytical, Inc., Chelmsford, MA, USA).

2.6. High-resolution ^{13}solid-state spectroscopy (^{13}CP-MAS)

^{13}C CP-MAS spectra of precursor polymers were recorded using the ramp $^{1}H \rightarrow {}^{13}C$ CP-MAS (cross-polarization and magic angle spinning) sequence with proton decoupling during acquisition. All the solid-state Nuclear Magnetic Resonance (ss-NMR) experiments were performed at room temperature in a Bruker Avance II–300 spectrometer (Bruker BioSpin GmbH, Rheinstetten, Germany) equipped with a 4-mm MAS probe, using ZrO_2 rotors for CS and LMMDS. For the freeze-dried PECs, a ZrO_2 rotor with spacer was used. The operating frequency for protons and carbons was

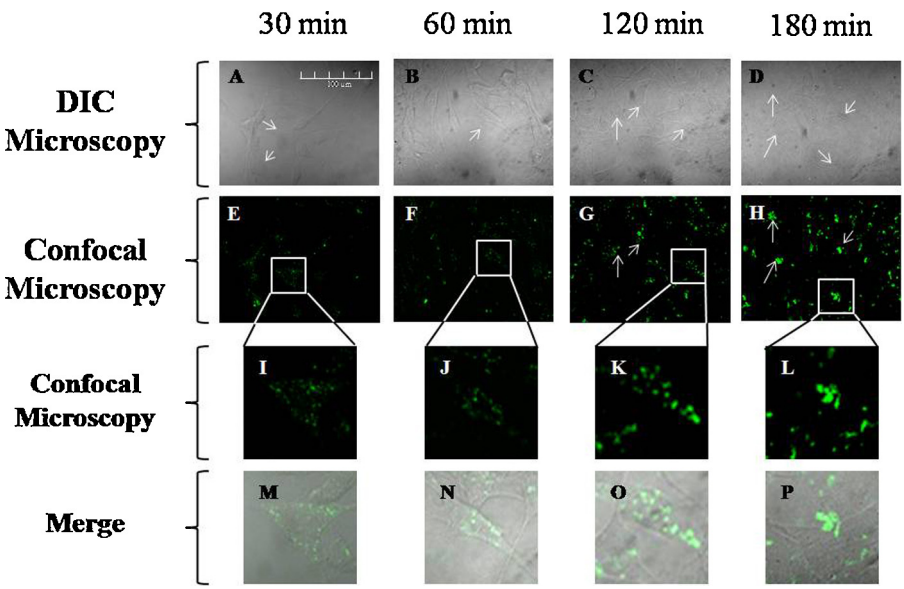

Fig. 4. H5 V cells incubated in the presence of FITC-labeled PECs (in a concentration equivalent to 10 μg/mL LMMDS) for 30, 60, 120 and 180 min. Differential interference contrast microscopy (DIC) images: 30 min (A), 60 min (B), 120 min (C) and 180 min (D). Confocal fluorescence microscopy images for FITC: 30 min (E), 60 min (F), 120 min (G) and 180 min (H). Amplification of E–H, focusing on one cell only (white boxes). Merge composites (DIC and confocal images): 30 min (M), 60 min (N), 120 min (O) and 180 min (P). White arrows indicate FITC-PECs interacting with the cells. Bar scale: 100 μm.

300.13 and 75.46 MHz, respectively. Glycine was used as an external reference for the ^{13}C spectra and to set the Hartmann–Hahn matching condition in the cross-polarization experiments. The recycling time was 4 s and the contact time during CP employed was 1.5 ms. The two-pulse phase modulation (TPPM) was used for heteronuclear decoupling during acquisition with a proton field H_{1H} satisfying $\omega_{1H}/2\pi = \gamma_H H_{1H} = 62$ kHz (Bennett, Rienstra, Auger, Lakshmi, & Griffin, 1995). The spinning rate for all the samples was 10 kHz. The number of scans was 20,000 for the freeze-dried CS-LMMDS PECs and 4000 for the rest of the solids studied.

2.7. Electrophoretic mobility of CS-LMMDS PECs

The electrophoretic mobility of CS-LMMDS PECs was estimated by running them in a 6% polyacrylamide gel electrophoresis (PAGE) as described previously (Rasente et al., 2012).

2.8. Cell culture

Cells derived from polyoma middle T-transformed murine heart endothelium (H5V) (Calabrese et al., 2011) were grown in DMEM supplemented with 10% FBS, streptomycin (100 mg/mL) and penicillin (100 UI/mL) in 5% CO_2 atmosphere, at 37 °C. The medium was exchanged every 48 h until the cells reached 70–80% confluence.

The macrophage cell line Raw 264.7 (Abelson murine leukemia virus-transformed cells) was a gift by Prof. Juliana Leoni. Culture conditions for Raw 264.7 cells were the same as those for H5V cells. For both cell types, cell viability was studied using the Trypan Blue exclusion method.

2.9. MTT assay

H5V cells were cultured in the absence or in the presence of increasing doses of LMMDS (0–50 μg/mL), CS (0–50 μg/mL), or PEC suspension (0–20 μg/mL, according to their LMMDS concentration), for 3 h. Following the manufacturer's instructions, we used the 3-(4,5-dimethylthiazol-2-yl)-2,-5-diphenyltetrazolium bromide (MTT) assay (Promega Corp., Madison, WI, USA) to evaluate the activity of the mitochondria respiratory chain as an indicator of the number of viable cells (Galluzzi et al., 2009). All experiments were performed in triplicate and results expressed as mean ± SD.

2.10. PECs uptake

H5V cells and Raw 264.7 cells grown separately on coverslips were incubated in the presence of FITC-PECs (10 μg/mL, according to their LMMDS concentration) for 30, 60, 120 and 180 min, and then fixed in 4% paraformaldehyde for 20 min. Fluorescence and differential interference contrast microscopy (DIC) images were taken with Nikon Microscope (Eclipse Ti, Nikon Instruments, Melville, NY, USA), using the software Micrometrics SE Premium, and processed with BioimageXD 1.0 software. Images of confocal fluorescence were obtained by an Olympus FV300 confocal laser scanning microscope (model BX61, Olympus Corp., Tokyo, Japan) equipped with Ar and He–Ne lasers, and oil immersion 60X numerical aperture 1.4. Images were taken with the acquisition software FluoView version 3.3. A minimum of 10 fields containing several cells were collected from each sample. Optical sections of 0.5 μm were obtained. Images were analyzed using ImageJ and Image-Pro plus version 4.5.

To confirm selective uptake, both cell types (H5V and Raw 264.7 cell lines) were grown together on coverslips. Equal number of each type of cell was co-cultured, in the same culture conditions as described above (Section 2.8). These co-culture coverslips were incubated in the presence of FITC-PECs (10 μg/mL, according to their LMMDS concentration) for 30 min, and then fixed in 4% paraformaldehyde for 20 min. Fluorescence and DIC microscopy images were obtained and analyzed as described above (Section 2.10).

2.11. PECs retention time

H5V cells grown on coverslips were incubated in the presence of FITC-PECs (10 μg/mL, according to their LMMDS concentration) for 30 min, and then washed twice with sterile phosphate buffer solution pH 7.2–7.4 to eliminate the excess of PECs that were not entrapped by the cells. After washing, H5V cells were incubated with DMEM supplemented medium without SFB for 30, 60, 90, 120 and 180 min; and then fixed in 4% paraformaldehyde for 20 min.

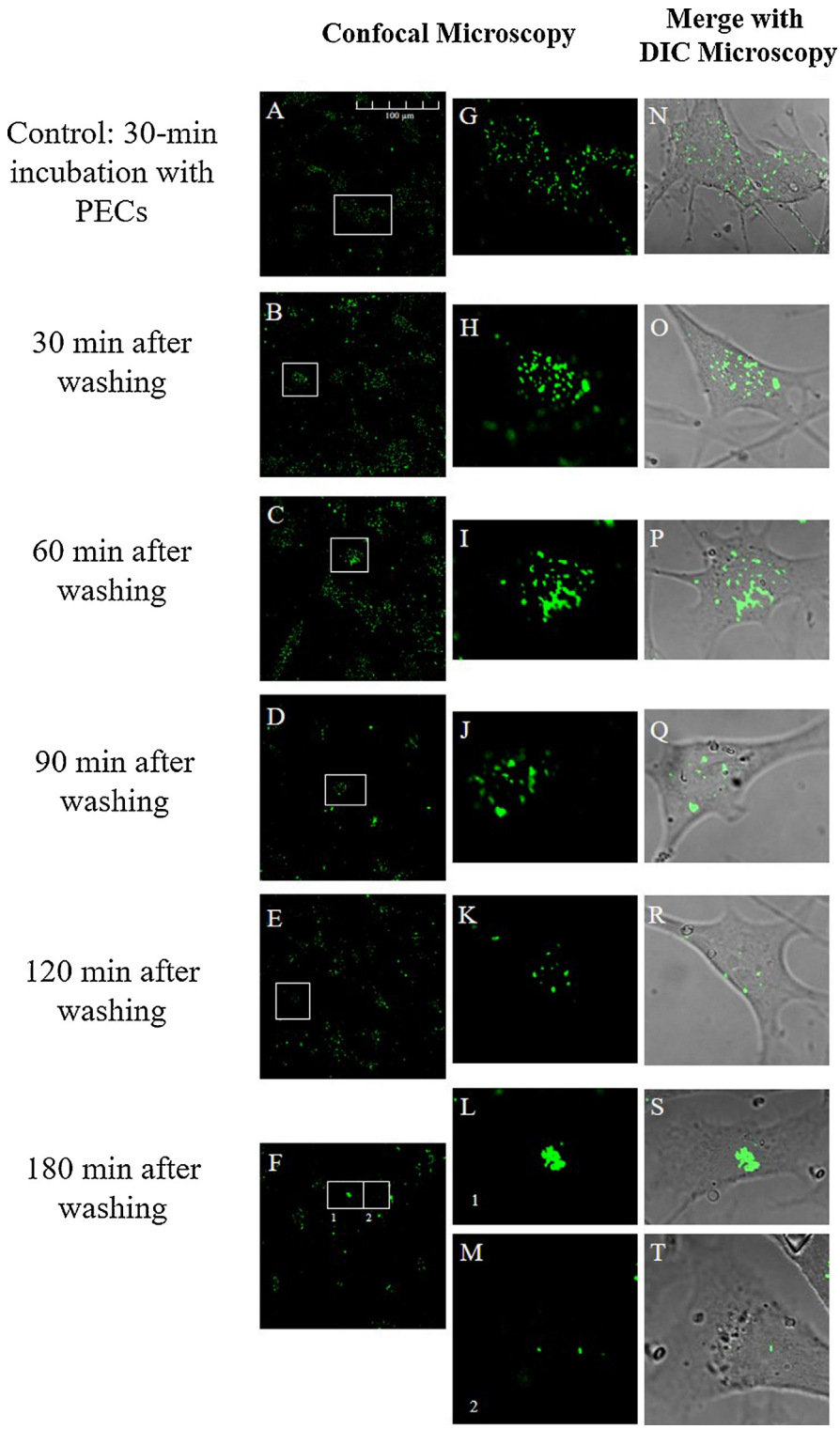

Fig. 5. PECs retention time by H5 V cells. H5 V cells incubated in the presence of FITC-PECs (in a concentration equivalent to 10 μg/mL LMMDS) for 30 min, then washed to eliminate the excess of PECs, and incubated with DMEM for 30, 60, 90, 120 and 180 min. Confocal fluorescence microscopy images for FITC: Control −30 min in the presence of PECs—(A), 30 min after washing (B), 60 min after washing (C), 90 min after washing (D), 120 min after washing (E) and 180 min after washing (F). Amplification of G–M, focusing on one cell only (white boxes). Merge composites (DIC and confocal images): Control −30 min in the presence of PECs– (N), 30 min after washing (O), 60 min after washing (P), 90 min after washing (Q), 120 min after washing (R) and 180 min after washing (S and T). Bar scale: 100 μm.

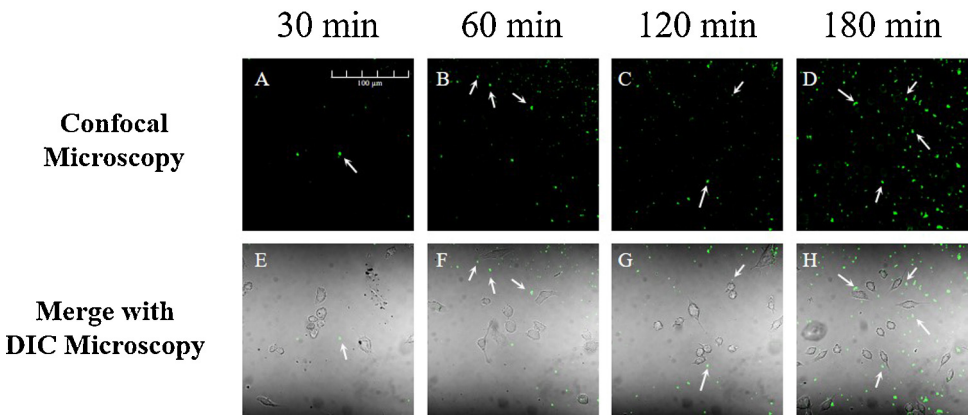

Fig. 6. Raw 264.7 cells incubated in the presence of FITC-labeled PECs (in a concentration equivalent to 10 μg/mL LMMDS) for 30, 60, 120 and 180 min. Fluorescence microscopy images for FITC: 30 min (A), 60 min (B), 120 min (C) and 180 min (D). Merge composites (DIC and fluorescence images): 30 min (E), 60 min (F), 120 min (G) and 180 min (H). White arrows indicate PECs-FITC, which, if present, were mainly located outside the cells. Bar scale: 100 μm.

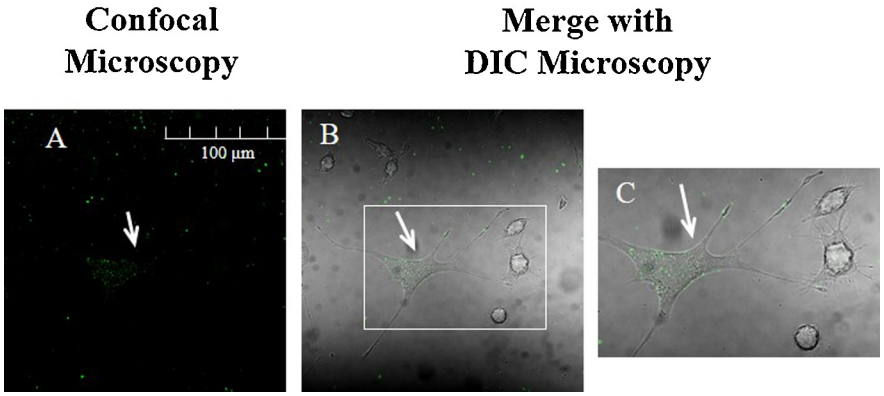

Fig. 7. H5V cells and Raw 264.7 cells co-cultured and incubated in the presence of FITC-labeled PECs (in a concentration equivalent to 10 μg/mL LMMDS) for 30 min. (A) Fluorescence microscopy image for FITC. (B) Merge composite (DIC and fluorescence images). (C) Amplification of (B), focusing on one endothelial cell and three macrophages (white box in B). The white arrow indicate the uptake of PECs-FITC by the endothelial cell H5V. Bar scale: 100 μm.

Fluorescence and DIC microscopy images were obtained and analyzed as described above (Section 2.10).

2.12. Statistical analysis

Data are expressed as mean ± SD. The statistical analysis was performed with the *t*-Student test or a two-way ANOVA and Bonferroni's test (Graph Pad Prism 5 software). Values of $p < 0.05$ were considered significantly different from controls.

3. Results

3.1. Production and characterization of CS-LMMDS PECs

CS-LMMDS PECs were produced by the ionotropic gelification method (Liu, Jiao, Wang, Zhou, & Zhang, 2008) using CS of low and high molecular weight. The PECs obtained with low molecular weight CS exhibited a bimodal size distribution with a major peak of 729 ± 11 nm (93%) and a minor one of 91 ± 11 nm (7%), the PDI value being 0.322 ± 0.055. When CS of higher molecular weight was used, a highly polydisperse suspension (PDI = 0.706 ± 0.120) showing three size populations in the range of 1130–2345 nm (60–71%), 156–360 nm (20–31%) and 27–60 nm (9%) was obtained. In all cases, the Z-potential of the PECs was highly positive (>+49 mV). Based on these findings, our studies employed low molecular weight CS. Then, the physical stability of CS-LMMDS PECs was analyzed upon storage over 14 days at room temperature. PECs remained unaltered (Table 1).

3.2. Composition of the PECs

To estimate the ratio between both polyelectrolytes in the PECs, samples were primarily analyzed by elemental analysis (Table 2). LMMDS was the only polyelectrolyte that contributed to the sulfur content (%S) in the PECs composition. The ratio between S/N in LMMDS starting material was 2.15, while in the PECs that ratio was 0.19, indicating that LMMDS was the minor component. Then, it was possible to discriminate the amount of each polymer through the total nitrogen content ($\%N_{total}$) calculated according to Eq. (1):

$$\%N_{total} = \%N_{CS} + \%N_{LMMDS} \quad (1)$$

where $\%N_{CS}$ and $\%N_{LMMDS}$ are the %N in CS and LMMDS, respectively.

Since the %N for LMMDS in the PECs was 0.45, and employing the same S:N ratio described both for LMMDS starting material and for PECs, it was established that the relative CS:LMMDS weight content was approximately 9:1.

The ^{13}C CP-MAS spectra for each polyelectrolyte (CS and LMMDS), a CS:LMMDS physical blend (1:1 and 9:1) and freeze-dried PECs are shown in Fig. 1. The assignment of the ^{13}C resonance signals was done according to previous descriptions performed for LMMDS and CS (Fig. 1A and B, respectively; see Reference scheme

in Fig. 1) (De Angelis, Capitani, & Crescenzi, 1998; Winter, Taylor, Stevens, Morris, & Rees, 1986). As seen in Fig. 1C, the ^{13}C CP-MAS spectrum for the 1:1 physical blend was the result of the sum of the resonance signals obtained separately for each of the compounds. On the other hand, the ^{13}C CP-MAS spectrum for the 9:1 mixture showed only signals from the major component in the blend (Fig. 1D). Conversely, the ^{13}C CP-MAS spectrum of the PECs showed significant changes with respect to the spectrum obtained for the physical mixture and each individual precursor (Fig. 1). Unmodified characteristic signals at 50.9 ppm for LMMDS (>CH-NH-acetyl, ^{B}C, LMMDS) and 57.3 ppm for CS (>CH-NH2, ^{2}C) confirmed the presence of LMMDS and CS in the PECs (Fig. 1E). On the other hand, in the PECs a significant shift of the characteristic peaks of LMMDS from ~175 ppm (Fig. 1A) to approximately 185 ppm was evident (Fig. 1E). Moreover, the signals at 68.2 ppm (^{L}C and ^{I}C) of LMMDS (Fig. 1A) and 82.8 ppm (^{4}C) of CS (Fig. 1B) completely disappeared in the particles (Fig. 1E).

3.3. Electrophoretic mobility assays

The electrophoretic mobility of CS-LMMDS PECs was compared with the mobility of the starting material LMMDS by PAGE analysis. Results showed the characteristic broad and diffuse band for a DS solution, which reflects a broad range of molecular weights for the GAG, and a diffuse band of lower molecular weight corresponding to the starting LMMDS solution (Fig. 2). In contrast, after filtration, PECs showed a well-defined band (Fig. 2).

3.4. CS-LMMDS PECs' uptake by endothelial cells

Initially, we evaluated the number of viable endothelial cells in the presence of the PECs. H5V cells were incubated in the absence (control) or in the presence of increasing PEC concentrations (according to the concentration of LMMDS in the PECs). Results indicated no statistical difference in the number of viable cells with respect to the control after the addition of 5–20 μg/mL PECs (Fig. 3). In addition, nontoxicity for high doses (50 μg/mL) of LMMDS or CS was registered (Fig. 3).

Once the nontoxicity of the PECs was established, their uptake by microvascular ECs was studied by microscopy employing FITC-labeled PECs. The concentration of PECs in this experiment was equivalent to the biologically active concentration of LMMDS, 10 μg/mL (Rasente et al., 2012).

Control H5V cells in the absence of PECs showed the typical spread morphology with lamellipodia that was maintained throughout the experiment (data not shown). Fig. 4E–H show the confocal laser microscopy images of FITC-PECs uptaken by H5V cells after 30, 60, 120 or 180 min of incubation, respectively. After 30 and 60 min of incubation, cells presented a homogeneous green dotted signal. As the incubation time increased (120 and 180 min), FITC-PECs were restricted to certain areas of the cells, as confirmed by merge images of the single cells (Fig. 4M–P). Fig. 4I–L show an enlarged image of each condition, displaying one cell only.

Furthermore, we assessed the retention time of PECs by H5V. Cells were incubated 30 min in the presence of PECs, washed and then incubated in DMEM for 30, 60, 90, 120 or 180 min (Fig. 5). Fluorescence was observed by confocal laser microscopy throughout the incubation time points (Fig. 5A–F). Nevertheless, the homogeneous green dotted signal changed progressively to a restrictive localization to certain areas of the cells (Fig. 5G–M and N–T). Finally, only few cells showed an accumulative fluorescence 180 min after washing (Fig. 5S and T).

On the other hand, when another cell type (Raw 264.7 cells) was cultured in the presence of FITC-PECs, cellular uptake was not detected in each time analyzed (Fig. 6A–D). In this case, FITC-PECs, when present, localized outside the cells (Fig. 6E–H).

In order to confirm the specific uptake of FITC-PECs by ECs, co-cultures between H5V and Raw 264.7 were performed. The homogeneous green dotted signal was only detectable in the ECs characterized by their typical spread morphology (Fig. 7B and C). On the other hand, no fluorescence was detected in Raw 264.7 cells.

4. Discussion

PEC-based nano- and submicron biomaterials represent a very promising platform for the prevention, diagnosis and treatment of vascular pathologies (Wen et al., 2012). CS is a natural biopolymer, widely utilized in PEC formation for delivery of therapeutic compounds (Hansson et al., 2012). In this work, we investigated the development of LMMDS-loaded PECs as a strategy to selectively target the vascular endothelium. For this, LMMDS was complexed with CS to form physically stable submicron particles and the cellular uptake of this complex by vascular ECs was characterized.

LMMDS, obtained by peroxy-radical depolymerization from a parental bovine DS of ~60, is a biomaterial with a molecular weight of ~5 kDa; this GAG preserves the sulfated sequences (2-*O*-sulfation of the iduronic acid units and/or 4 or 6 positions of glucosamine N acetyl) that are essential for DS-heparin cofactor II interaction (Alberto, Giaquinta Romero, Lazzari, & Calabrese, 2008). As we have previously reported, 10 μg/mL of LMMDS induces the entrance of the endothelial cells into S phase of the cell cycle, enhances the activity of MMP2, and might modulate cell migration of ECs, through mechanisms independent of TNF-α autocrine regulation (Rasente et al., 2012).

The properties of CS-GAG PECs significantly depend on the preparation conditions, such as the charge ratios (polycation/polyanion ratio), ionic strength, and pH (Seyrek & Dubin, 2010). Here, the formation of CS-LMMDS PECs was ensured by choosing a pH of 3.5 whereby the amine groups of CS ($pK_a \sim 6$) were protonated and the carboxylic groups of LMMDS ($pK_a \sim 1.8$) available as negatively-charged carboxylates. Beyond the strong electrostatic interactions between both components, additional inter-macromolecular bonds such as hydrogen bonding, van der Waals, dipole-dipole and hydrophobic interactions could not be ruled out (Koetz & Kosmella, 2007).

The size of the particles is important in the promotion of cell binding and internalization; usually the smaller the size, the greater the cell internalization (Desai, Labhasetwar, Walter, Levy, & Amidon, 1997; Foged, Brodin, Frokjaer, & Sundblad, 2005; Panyam & Labhasetwar, 2003; Rejman, Oberle, Zuhorn, & Hoekstra, 2004). Thus, the effect of the molecular weight of CS on the size of the particles was initially assessed (Liu et al., 2008). High molecular weight CS was substantially more viscous than the low molecular weight counterpart and led to the formation of large particles with a very high PDI of 0.706 ± 0.120. In contrast, low molecular weight CS resulted in PECs with sizes in the 695–730 nm range (Table 1). Overall, results suggested that the high molecular weight of the polymer did not allow the chain disentanglements that are necessary to form small particles instead of large particle clusters (Sæther, Holme, Maurstad, Smidsrød, & Stokke, 2008). Our results were in agreement with those described by Santander-Ortega that suggested the higher stability of nanocapsules formulated with low molecular weight CS (Santander-Ortega, Peula-García, Goycoolea, & Ortega-Vinuesa, 2011). In addition, the interaction of CS and LMMDS in the particles was confirmed by a comparative ^{13}C CP-MAS analysis of the pure polymeric precursors, CS/LMMDS physical blends, and freeze-dried particles.

Repulsive forces are a key player in the stabilization of CS particles in biological media (Santander-Ortega et al., 2011). The PECs showed a very positive Z-potential (+49 mV) due to a CS excess in the composition (Table 2) that resulted in unaltered proper-

ties and no sedimentation even after storage over two weeks. Moreover, these results supported that CS did not undergo neither oxidation, a phenomenon that increases the concentration of carboxylate groups and leads to a gradual decrease of the Z-potential (Jonassen, Kjøniksen, & Hiorth, 2012), nor depolymerization, which is observed as a size decrease (Morris, Castile, Smith, Adams, & Harding, 2011).

Normal adult endothelium is considered to be in a quiescent state, although being metabolically active. ECs respond to diverse paracrine, autocrine and endocrine signals with changes in cell surface protein expression and mediator secretion that allow the endothelium to regulate a range of pathophysiological processes. Endothelial dysfunction has been observed in patients with atherosclerosis, hyperlipidemia, diabetes, hypertension, aging, and obesity (Hadi, Carr, & Suwaidi, 2005; Rajendran et al., 2013; Sima, Stancu, & Simionescu, 2009). Our study showed the uptake of CS-LMMDS PECs by microvascular ECs, but not by a different cell line, such as Raw 264.7. The retention of the PECs by ECs over at least 2 h is primarily relevant for diagnostic applications. Furthermore, in therapeutic interventions where an active payload inhibits a specific cellular pathway (e.g., expression of a specific gene or protein) in a more permanent manner (for several hours or days), this targeting strategy would probably result in a more efficient outcome than a non-targeted approach. Then, based on the prolongation of the pharmacological effect of the cargo, the administration frequency should be adjusted. Thus, the relatively short residence time should not be understood as a critical drawback but as a limitation that could be overcome with additional design of the nanoparticles by for example changing the content of DS. It is also noteworthy that under the experimental conditions of the study, CS and CS-LMMDS PECs did not affect the mitochondrial respiratory chain, as shown through the MTT assay; therefore, the acute cell necrosis with mitochondrial damage described for other cationic microcarriers is probably absent (Wei et al., 2015). Considering that low molecular weight CS is a useful carrier for molecular drugs, the addition of a small payload of LMMDS (10% w/w) enabled not only the targeting of the PECs to ECs but also might capitalize on the pharmacodynamics of the particles due to the known biological activity of LMMDS on this cell type. For example, DS chains greatly increase the rate of thrombin inhibition by Heparin Cofactor II. Since thrombin is thought to contribute to atherogenesis by influencing coagulation, chemoattraction and cell proliferation, DS would provide the tissue with antiatherogenic properties (Rasente et al., 2012; Tollefsen, 2010). Moreover, LMMDS induces the entrance of cells into the S phase of the cell cycle, enhances the activity of MMP2, and might modulate endothelial cell migration through mechanisms independent of TNF-α (Rasente et al., 2012). At the same time, it is important to highlight the antioxidant activity of CS owing to the strong hydrogen-donating ability of the polymer, activity that has been described by Younes and Rinaudo (2015).

5. Conclusion

This study described an easy and reproducible method to produce a novel nanoparticulate system of low molecular weight CS-LMMDS that provides a unique combination of biological features such as endothelial cell binding, antioxidant activity, cell entrance into the S phase of the cell cycle, enhancement of the activity of MMP2, and the possible control of endothelial cell migration. Ongoing studies are oriented to establish the molecular pathways behind this specific recognition and explore the capacity of CS-LMMDS PECs to distinguish between a quiescent and an injured endothelium, a stage that will be crucial to apply them in the prevention, diagnosis and therapy of vascular disease.

Author contributions

The manuscript was written through contributions of all authors. All authors have given approval to the final version of the manuscript.

Acknowledgements

The authors acknowledge the financial support of the University of Buenos Aires (Grant # 20020130100626BA) and thank Prof. Dr. Juliana Leoni (IDEHU, School of Pharmacy and Biochemistry, University of Buenos Aires) for kindly donating the Raw 264.7 cells used in the experiments.

References

Agnihotri, S. A., Mallikarjuna, N. N., & Aminabhavi, T. M. (2004). Recent advances on chitosan-based micro- and nanoparticles in drug delivery. *Journal of Controlled Release*, *100*(1), 5–28. http://dx.doi.org/10.1016/j.jconrel.2004.08.010

Alberto, M. F., Giaquinta Romero, D., Lazzari, M., & Calabrese, G. C. (2008). Antithrombotic and anticomplementary properties of a very low molecular mass dermatan sulfate. *Thrombosis Research*, *122*(1), 109–116. http://dx.doi.org/10.1016/j.thromres.2007.09.001

Anggraeni, V. Y., Emoto, N., Yagi, K., Mayasari, D. S., Nakayama, K., Izumikawa, T., et al. (2011). Correlation of C4ST-1 and ChGn-2 expression with chondroitin sulfate chain elongation in atherosclerosis. *Biochemical and Biophysical Research Communications*, *406*(1), 36–41. http://dx.doi.org/10.1016/j.bbrc.2011.01.096

Bennett, A. E., Rienstra, C. M., Auger, M., Lakshmi, K. V., & Griffin, R. G. (1995). Heteronuclear decoupling in rotating solids. *The Journal of Chemical Physics*, *103*(16), 6951. http://dx.doi.org/10.1063/1.470372

Calabrese, G. C., Alberto, M. F., Tubio, R., Marani, M. M., Fernández De Recondo, M. E., Lazzari, M., et al. (2004). A small fraction of dermatan sulfate with significantly increased anticoagulant activity was selected by interaction with the first complement protein. *Thrombosis Research*, *113*(3–4), 243–250. http://dx.doi.org/10.1016/j.thromres.2004.01.014

Calabrese, G. C., Gazzaniga, S., Oberkersch, R., & Wainstok, R. (2011). Decorin and biglycan expression: its relation with endothelial heterogeneity. *Histology and Histopathology*, *26*, 481–490.

De Angelis, A. A., Capitani, D., & Crescenzi, V. (1998). Synthesis and ^{13}C CP-MAS NMR characterization of a new chitosan-based polymeric network. *Macromolecules*, *31*, 1595–1601.

Desai, M. P., Labhasetwar, V., Walter, E., Levy, R. J., & Amidon, G. L. (1997). The mechanism of uptake of biodegradable microparticles in Caco-2 cells is size dependent. *Pharmaceutical Research*, *14*(11), 1568–1573.

Díaz, V. B., Dománico, R. H., & Fussi, F. (1990). US. Patent 4977250.

Díaz, V. B., Dománico, R. H., & Fussi, F. (1993). European Patent.

Foged, C., Brodin, B., Frokjaer, S., & Sundblad, A. (2005). Particle size and surface charge affect particle uptake by human dendritic cells in an in vitro model. *International Journal of Pharmaceutics*, *298*(2), 315–322. http://dx.doi.org/10.1016/j.ijpharm.2005.03.035

Fogelstrand, P., & Borén, J. (2012). Retention of atherogenic lipoproteins in the artery wall and its role in atherogenesis. *Nutrition, Metabolism, and Cardiovascular Diseases: NMCD*, *22*(1), 1–7. http://dx.doi.org/10.1016/j.numecd.2011.09.007

Galluzzi, L., Aaronson, S., Abrams, J., Alnemri, E., Andrews, D., Baehrecke, E., et al. (2009). Guidelines for the use and interpretation of assays for monitoring cell death in higher eukaryotes. *Cell Death & Differentiation*, *16*(8), 1093–1107. http://dx.doi.org/10.1038/cdd.2009.44

Hadi, H. A., Carr, C. S., & Al Suwaidi, J. (2005). Endothelial dysfunction: cardiovascular risk factors, therapy, and outcome. *Vascular Health and Risk Management*, *1*(3), 183–198.

Hansson, A., Di Francesco, T., Falson, F., Rousselle, P., Jordan, O., & Borchard, G. (2012). Preparation and evaluation of nanoparticles for directed tissue engineering. *International Journal of Pharmaceutics*, *439*(1–2), 73–80. http://dx.doi.org/10.1016/j.ijpharm.2012.09.053

Jackson, K. G., Poppitt, S. D., & Minihane, A. M. (2012). Postprandial lipemia and cardiovascular disease risk: interrelationships between dietary, physiological and genetic determinants. *Atherosclerosis*, *220*(1), 22–33. http://dx.doi.org/10.1016/j.atherosclerosis.2011.08.012

Jonassen, H., Kjøniksen, A., & Hiorth, M. (2012). Stability of chitosan nanoparticles cross-linked with tripolyphosphate. *Biomacromolecules*, *13*, 3747–3756.

Koetz, J., & Kosmella, S. (2007). In H. G. Barth, & H. Pasch (Eds.), *Polyelectrolytes and nanoparticles*. Berlin: Springer.

Lacroix, S., Des Rosiers, C., Tardif, J. C., & Nigam, A. (2012). The role of oxidative stress in postprandial endothelial dysfunction. *Nutrition Research Reviews*, *25*(2), 288–301. http://dx.doi.org/10.1017/S0954422412000182

Little, P. J., Ballinger, M. L., & Osman, N. (2007). Vascular wall proteoglycan synthesis and structure as a target for the prevention of atherosclerosis. *Vascular Health and Risk Management*, *3*(1), 117–124. Retrieved from. http://www.pubmedcentral.nih.gov/articlerender.fcgi?artid=1994044&tool=pmcentrez&rendertype=abstract

Little, P. J., Chait, A., & Bobik, A. (2011). Cellular and cytokine-based inflammatory processes as novel therapeutic targets for the prevention and treatment of atherosclerosis. *Pharmacology & Therapeutics*, *131*(3), 255–268. http://dx.doi.org/10.1016/j.pharmthera.2011.04.001

Liu, Z., Jiao, Y., Wang, Y., Zhou, C., & Zhang, Z. (2008). Polysaccharides-based nanoparticles as drug delivery systems. *Advanced Drug Delivery Reviews*, *60*(15), 1650–1662. http://dx.doi.org/10.1016/j.addr.2008.09.001

Luo, Y., & Wang, Q. (2014). Recent development of chitosan-based polyelectrolyte complexes with natural polysaccharides for drug delivery. *International Journal of Biological Macromolecules*, *64*, 353–367. http://dx.doi.org/10.1016/j.ijbiomac.2013.12.017

Morris, G. A., Castile, J., Smith, A., Adams, G. G., & Harding, S. E. (2011). The effect of prolonged storage at different temperatures on the particle size distribution of tripolyphosphate (TPP)—chitosan nanoparticles. *Carbohydrate Polymers*, *84*(4), 1430–1434. http://dx.doi.org/10.1016/j.carbpol.2011.01.044

Nakashima, Y., Fujii, H., Sumiyoshi, S., Wight, T. N., & Sueishi, K. (2007). Early human atherosclerosis: accumulation of lipid and proteoglycans in intimal thickenings followed by macrophage infiltration. *Arteriosclerosis, Thrombosis, and Vascular Biology*, *27*(5), 1159–1165. http://dx.doi.org/10.1161/ATVBAHA.106.134080

Neufeld, E. B., Zadrozny, L. M., Phillips, D., Aponte, A., Yu, Z.-X., & Balaban, R. S. (2014). Decorin and biglycan retain LDL in disease-prone valvular and aortic subendothelial intimal matrix. *Atherosclerosis*, *233*(1), 113–121. http://dx.doi.org/10.1016/j.atherosclerosis.2013.12.038

Oberkersch, R., Maccari, F., Bravo, A. I., Volpi, N., Gazzaniga, S., & Calabrese, G. C. (2014). Atheroprotective remodelling of vascular dermatan sulphate proteoglycans in response to hypercholesterolaemia in a rat model. *International Journal of Experimental Pathology*, *95*, 181–190. http://dx.doi.org/10.1111/iep.12072

Panyam, J., & Labhasetwar, V. (2003). Biodegradable nanoparticles for drug and gene delivery to cells and tissue. *Advanced Drug Delivery Reviews*, *55*(3), 329–347. http://dx.doi.org/10.1016/S0169-409X(02)00228-4

Patel, M. P., Patel, R. R., & Patel, J. K. (2010). Chitosan mediated targeted drug delivery system: a review. *Journal of Pharmacy & Pharmaceutical Sciences*, *13*(3), 536–557.

Rajendran, P., Rengarajan, T., Thangavel, J., Nishigaki, Y., Sakthisekaran, D., Sethi, G., et al. (2013). The vascular endothelium and human diseases. *International Journal of Biological Sciences*, *9*(10), 1057–1069. http://dx.doi.org/10.7150/ijbs.7502

Ranney, D., Antich, P., Dadey, E., Mason, R., Kulkarni, P., Singh, O., et al. (2005). Dermatan carriers for neovascular transport targeting, deep tumor penetration and improved therapy. *Journal of Controlled Release*, *109*(1–3), 222–235. http://dx.doi.org/10.1016/j.jconrel.2005.09.022

Rasente, R. Y., Egitto, P., & Calabrese, G. C. (2012). Low molecular mass dermatan sulfate modulates endothelial cells proliferation and migration. *Carbohydrate Research*, *356*, 233–237. http://dx.doi.org/10.1016/j.carres.2012.03.036

Rejman, J., Oberle, V., Zuhorn, I. S., & Hoekstra, D. (2004). Size-dependent internalization of particles via the pathways of clathrin- and caveolae-mediated endocytosis. *The Biochemical Journal*, *377*, 159–169.

Sæther, H. V., Holme, H. K., Maurstad, G., Smidsrød, O., & Stokke, B. T. (2008). Polyelectrolyte complex formation using alginate and chitosan. *Carbohydrate Polymers*, *74*(4), 813–821. http://dx.doi.org/10.1016/j.carbpol.2008.04.048

Santander-Ortega, M. J., Peula-García, J. M., Goycoolea, F. M., & Ortega-Vinuesa, J. L. (2011). Chitosan nanocapsules: effect of chitosan molecular weight and acetylation degree on electrokinetic behaviour and colloidal stability. *Colloids and Surfaces B: Biointerfaces*, *82*(2), 571–580. http://dx.doi.org/10.1016/j.colsurfb.2010.10.019

Sarmento, B., Ribeiro, A., Veiga, F., & Ferreira, D. (2006). Development and characterization of new insulin containing polysaccharide nanoparticles. *Colloids and Surfaces B: Biointerfaces*, *53*(2), 193–202. http://dx.doi.org/10.1016/j.colsurfb.2006.09.012

Seyrek, E., & Dubin, P. (2010). Glycosaminoglycans as polyelectrolytes. *Advances in Colloid and Interface Science*, *158*(1–2), 119–129. http://dx.doi.org/10.1016/j.cis.2010.03.001

Sima, A. V., Stancu, C. S., & Simionescu, M. (2009). Vascular endothelium in atherosclerosis. *Cell and Tissue Research*, *335*(1), 191–203. http://dx.doi.org/10.1007/s00441-008-0678-5

Sosnik, A., das Neves, J., & Sarmento, B. (2014). Mucoadhesive polymers in the design of nano-drug delivery systems for administration by non-parenteral routes: a review. *Progress in Polymer Science*, *39*(12), 2030–2075. http://dx.doi.org/10.1016/j.progpolymsci.2014.07.010

Thakker, S. P., Rokhade, A. P., Abbigerimath, S. S., Iliger, S. R., Kulkarni, V. H., More, U. A., et al. (2014). Inter-polymer complex microspheres of chitosan and cellulose acetate phthalate for oral delivery of 5-fluorouracil. *Polymer Bulletin*, *71*(8), 2113–2131.

Theocharis, A. D., Theocharis, D. A., De Luca, G., Hjerpe, A., & Karamanos, N. K. (2002). Compositional and structural alterations of chondroitin and dermatan sulfates during the progression of atherosclerosis and aneurysmal dilatation of the human abdominal aorta. *Biochimie*, *84*, 667–674.

Tollefsen, D. M. (2010). Vascular dermatan sulfate and heparin cofactor II. *Progress in Molecular Biology and Translational Science*, *93*(10), 351–372. http://dx.doi.org/10.1016/S1877-1173(10)93015-9

Tovar, A. M. F., Cesar, D. C. F., Leta, G. C., & Mourao, P. A. S. (1998). Age-related changes in populations of aortic glycosaminoglycans: species with low affinity for plasma low-density lipoproteins, and not species with high affinity, are preferentially affected. *Arteriosclerosis, Thrombosis, and Vascular Biology*, *18*(4), 604–614. http://dx.doi.org/10.1161/01. ATV.18.4.604

Trowbridge, J. M., & Gallo, R. L. (2002). Dermatan sulfate: new functions from an old glycosaminoglycan. *Glycobiology*, *12*(9), 117R–125R. Retrieved from. http://www.ncbi.nlm.nih.gov/pubmed/12213784

Wei, X., Shao, B., He, Z., Ye, T., Luo, M., Sang, Y., et al. (2015). Cationic nanocarriers induce cell necrosis through impairment of Na+/K+-ATPase and cause subsequent inflammatory response. *Cell Research*, *25*(2), 237–253. http://dx.doi.org/10.1038/cr.2015.9

Wen, Y., Grøndahl, L., Gallego, M. R., Jorgensen, L., Møller, E. H., & Nielsen, H. M. (2012). Delivery of dermatan sulfate from polyelectrolyte complex-containing alginate composite microspheres for tissue regeneration. *Biomacromolecules*, *13*, 905–917.

Wilson, B., Samanta, M. K., Santhi, K., Kumar, K. P. S., Ramasamy, M., & Suresh, B. (2010). Chitosan nanoparticles as a new delivery system for the anti-Alzheimer drug tacrine. *Nanomedicine: Nanotechnology, Biology, and Medicine*, *6*(1), 144–152. http://dx.doi.org/10.1016/j.nano.2009.04.001

Winter, W. T., Taylor, M. G., Stevens, E. S., Morris, E. R., & Rees, D. A. (1986). Solid-state ^{13}C NMR and X-ray diffraction of dermatan sulfate. *Biochemical and Biophysical Research Communications*, *137*(1), 87–93.

Younes, I., & Rinaudo, M. (2015). Chitin and chitosan preparation from marine sources. Structure, properties and applications. *Marine Drugs*, *13*(3), 1133–1174. http://dx.doi.org/10.3390/md13031133